

4 Results and discussion

In this chapter, the results are presented and discussed. First, the analysis of the visualization of turbulent drop breakup mechanisms in the RSM and in the orifice for different flow cases is presented. Then, stable drop diameter data for turbulent breakup of 5% O/W emulsions are correlated to a linear mechanistic model. The obtained model allow to estimate the maximum droplet size that will remain in equilibrium for a given energy dissipation rate.

4.1 Visualization of drop breakup in turbulent flow

This section presents the analysis of the drop breakup mechanisms for turbulent flow in a rotor – stator mixer and through an orifice in a pipe, acquired by visualization in a high-speed camera.

4.1.1 Drop breakup mechanisms in a rotor – stator mixer

The mechanisms responsible for drop breakup in a Rotor – Stator Mixer were studied by analysis of images obtained with a high-speed camera (2000 FPS). The principal case of analysis corresponded to fragmentation of an O/W emulsion with a content of 0.5% (V/V) of Drakeol 7 in tap water at a mixing speed of 6500 RPM ($Re = 20000$). Two main mechanisms were observed. The first one was a combination of the vortex produced by the circular motion of the rotor and the fluid jet generated in the stator holes; the second one was caused by the guillotine effect that droplets suffer in the rotor – stator gap.

The “vortex and jet” breakup mechanism is depicted in Figure 4.1. In it, the vortex created by circular motion of the rotor causes a preliminary breakup in the upper region of the vessel (Figure 4.1.a), wherein initially the low-density fluid lies (dispersed phase), generating larger spherical and non-spherical drops.

Then, the vortex redirects the droplets to a jet zone emerging from the stator holes. This jet is formed due to the collision of fluid on the leading edge of the stator hole walls, which converts tangential velocity, into radial velocity (Utomo, Baker and Pacek, 2009). As exposed by Calabrese et al. (2000), when the droplets reach the jet zone, they are exposed to the turbulent stress generated by the jet (Figure 4.1.b). Depending on the magnitude of the energy dissipation rate in the jet zone (proximity of the stator holes) and time scale (time in which the stress acts), the droplets can be deformed (Figure 4.1.c), and finally broken (Figure 4.1.d).

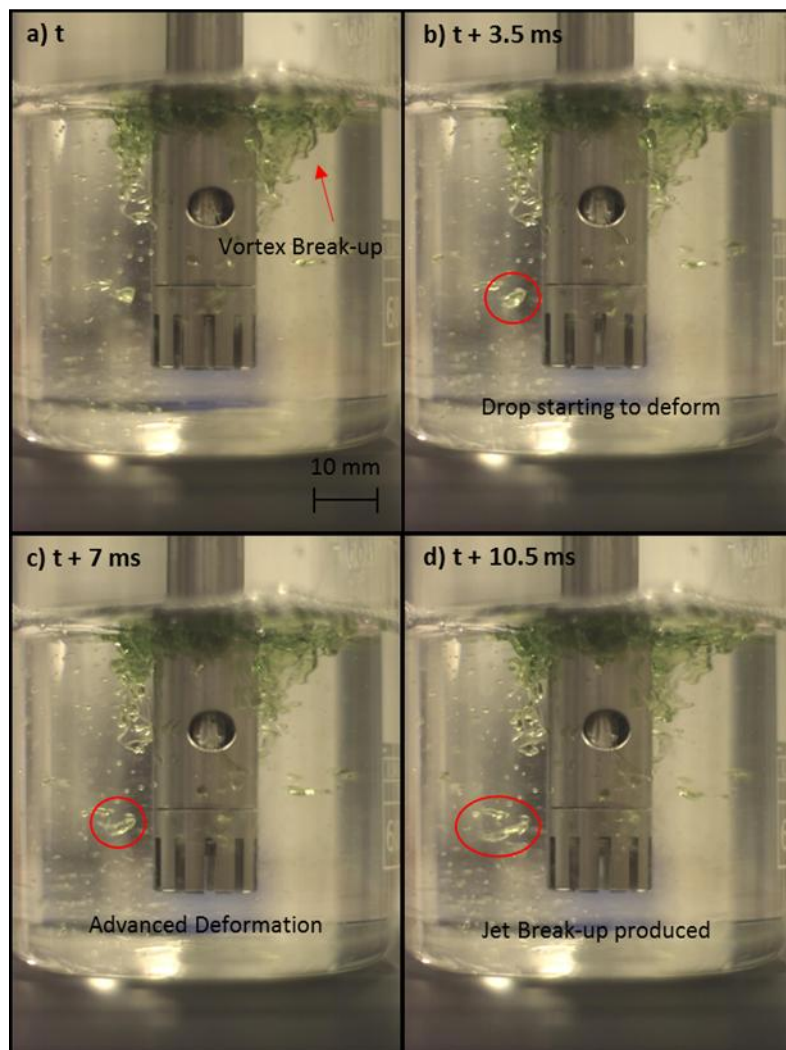


Figure 4. 1 Vortex and jet breakup mechanism in rotor – stator mixer. $\mu_d = 0.0178$ Pa.s, $\sigma = 17.65$ mN/m, $T = 25$ °C.

The second mechanism, the “mechanical” breakup mechanism is showed in Figure 4.2. Initially, droplets are entering into the rotor – stator system (Figure 4.2.a) from the gap region between the bottom of the vessel and the dispersing element, according to the standard flow pattern showed in Figure 4.3. Some

droplets enter directly to the rotor – stator gap, and some of them are deformed by impingement in the stator walls (Figure 4.2.b). When drops enter into the rotor – stator gap (Figure 4.2.c), they are subjected to high shear stresses produced by the velocity difference between the rotor and the stator. Finally, the droplets break into several fragments (Figure 4.2.d), which are expelled by the rotor – stator system through the jet zone previously described for the vortex and jet mechanism.

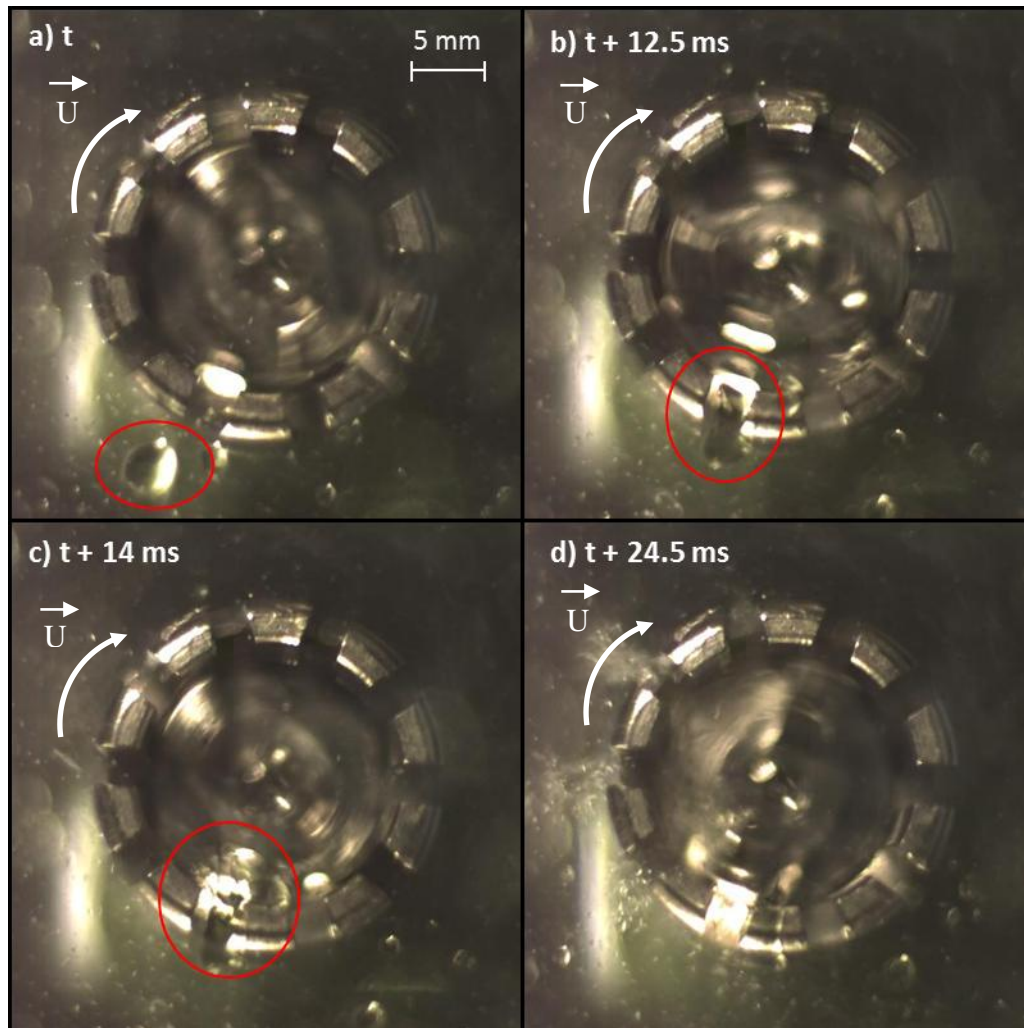


Figure 4. 2 Mechanical breakup mechanism in the rotor – stator mixer. $\mu_d = 0.0178$ Pa.s,
 $\sigma = 17.65$ mN/m, $T = 25$ °C.

It was not possible to determine which one is the dominant breakup mechanism, but from observations, it was perceived that the fragmentation rate in the mechanical mechanism is stronger than the fragmentation rate in the vortex and jet mechanism. Consequently, the mechanical mechanism is probably the responsible for produce the smallest droplets in the flow.

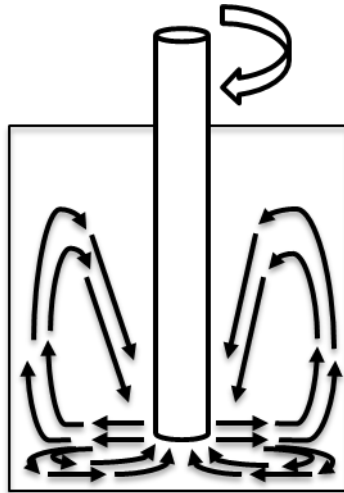


Figure 4. 3 Standard flow pattern in the high speed mixer.

4.1.1.1 Single droplet case

Various video samples were recorded to analyze the jet breakup mechanism for the case of a single droplet in the RSM. The results allowed the determination of individual effects of interfacial tension and dispersed phase viscosity on the breakup phenomenon. In all cases, the mixing speed and geometry were maintained fixed.

4.1.1.1.1 Effect of interfacial tension

Key moments for the single droplet breakup (jet mechanism) of mixing systems with high interfacial tension and low interfacial tension, are shown in Figures 4.4 and 4.5, respectively. As expected, it was observed that droplets were harder to deform in high interfacial tension systems. That occurs because in these systems, the high internal interfacial force which try to keep the drop spherical form, strongly opposes to the external stress, preventing the deformation of the droplets.

It was also observed a high fragmentation rate for droplets in low interfacial tension systems; consequently, small drop sizes and a large number of “daughter droplets” will be generated in the flow.

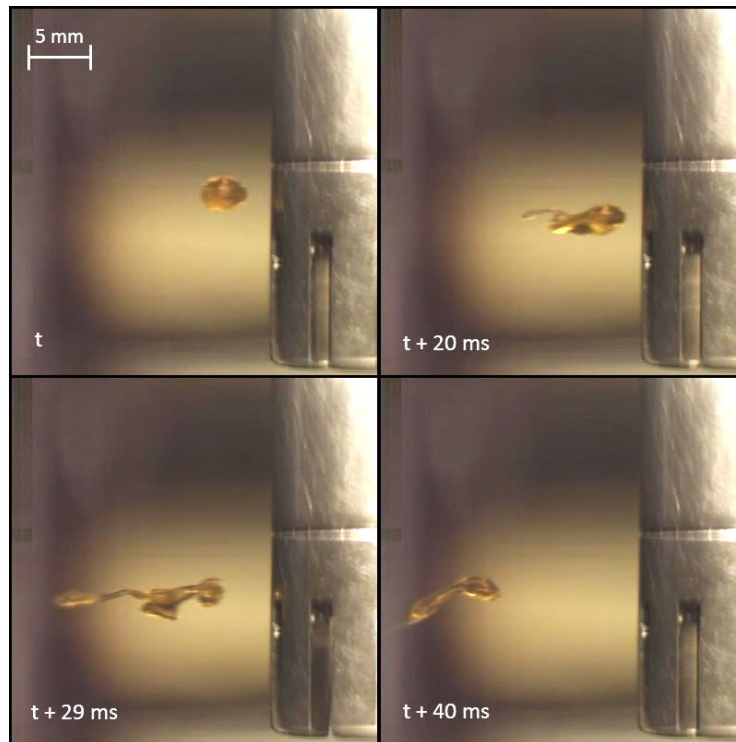


Figure 4. 4 Breakup of a single droplet in a rotor – stator Mixer. High interfacial tension case. $\mu_d = 0.192$ Pa.s, $\sigma = 24.51$ mN/m, $T = 25$ °C.

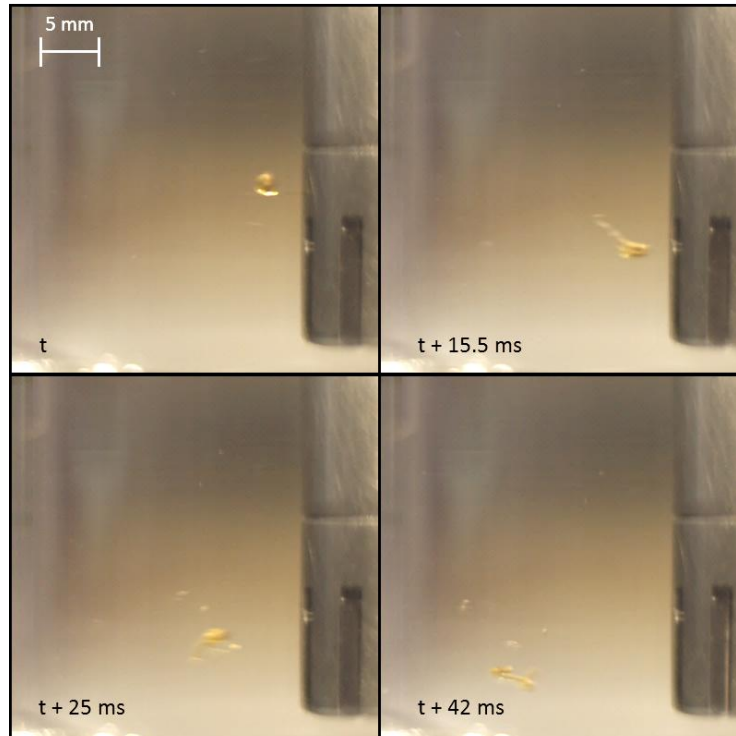


Figure 4. 5 Breakup of a single droplet in a rotor – stator mixer. Low interfacial tension case. $\mu_d = 0.192$ Pa.s, $\sigma = 1.79$ mN/m, $T = 25$ °C.

4.1.1.1.2 Effect of dispersed phase viscosity

The effect of the dispersed phase viscosity is shown in Figures 4.5 and 4.6 (Moderate viscosity oil and low viscosity oil, respectively). It is observed that, the more viscous droplets are capable of sustaining greater deformations prior to breakage and can stretch to larger lengths than less viscous droplets. Therefore, the required time scale to achieve the critical deformation and breakup is larger for high viscosity droplets. In addition, because of its high deformation resistance, viscous droplets have a low fragmentation rate.

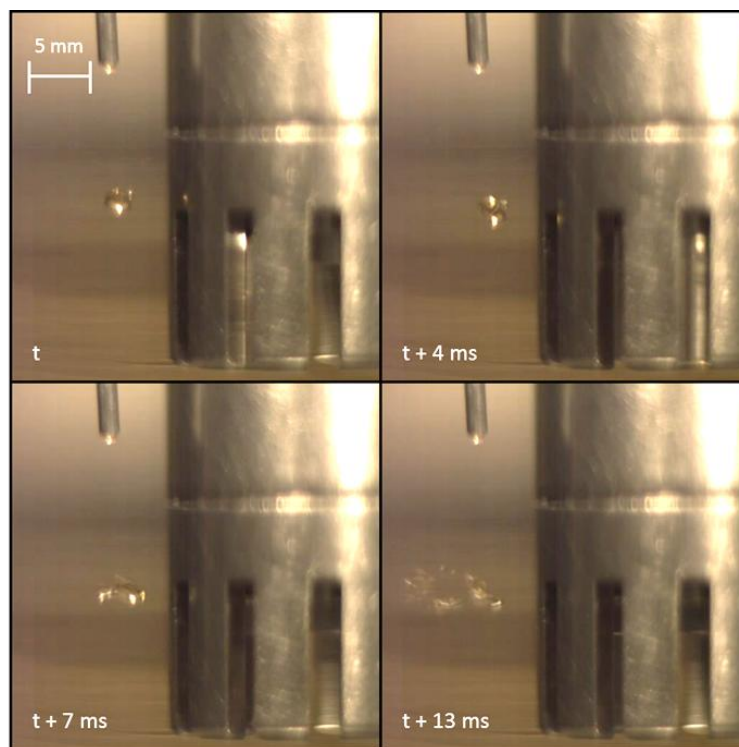


Figure 4. 6 Breakup of a single droplet in a rotor – stator mixer. Low dispersed phase viscosity case. $\mu_d = 0.0178$ Pa.s, $\sigma = 1.97$ mN/m, $T = 25$ °C.

The qualitative results are confirmed by the drop size distributions of emulsions obtained at the same mixing conditions, as shown in Figures 4.7 and 4.8. It is observed that the less viscous oil produces the emulsion with the smaller droplet size. In addition, the high fragmentation rates in the less viscous case generate a daughter droplet distribution more homogeneous than in the more viscous case, consequently, a more monodispersed drop size distribution is obtained.

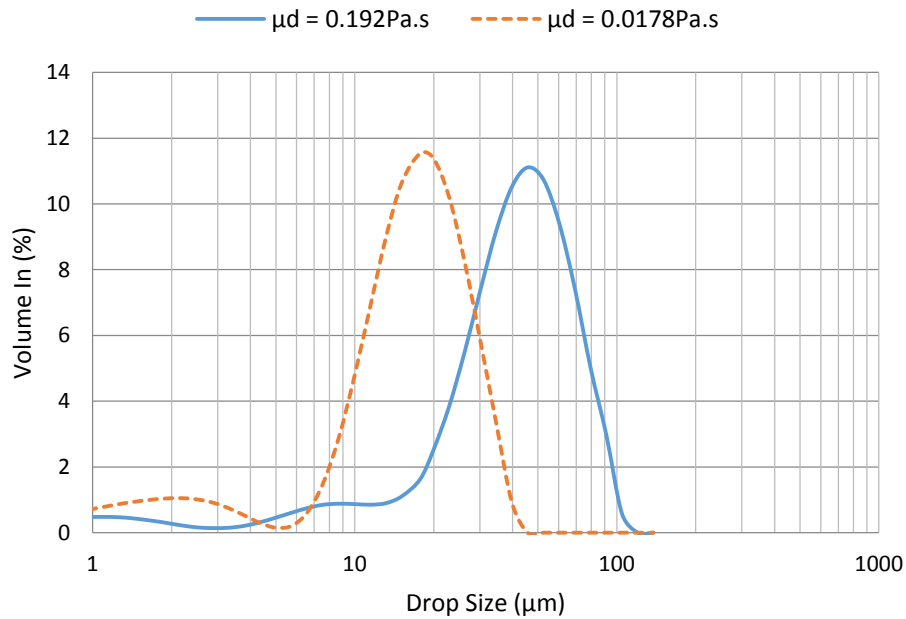


Figure 4. 7. Effect of dispersed phase viscosity on the drop size distribution of O/W emulsions. $\phi = 0.05$, $\sigma \sim 1.9$ mN/m, Mixing Time = 2 min, $Re = 27000$, $\epsilon = 46000$ W/Kg.

The same analysis is valid for higher Reynolds numbers (Figure 4.8), except that in the case of high Reynolds numbers, the distribution obtained for the less viscous oil is even more monodispersed.

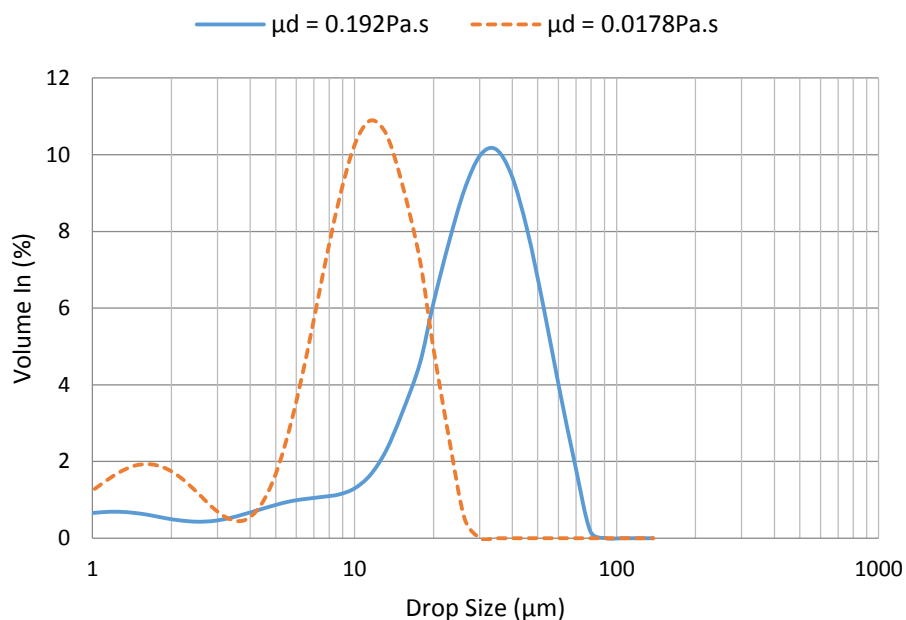


Figure 4. 8 Effect of dispersed phase viscosity on the drop size distribution of O/W emulsions. $\phi = 0.05$, $\sigma \sim 1.9$ mN/m, Mixing Time = 2 min, $Re = 50000$, $\epsilon = 290000$ W/Kg.

4.1.2 Drop breakup mechanisms through an orifice

The general features of the turbulent drop breakup process through an orifice were determined for different combinations of dispersed phase viscosity, interfacial tension and geometry of the orifice ($\beta = \text{Orifice Diameter}/\text{Pipe Diameter}$). Figures 4.9 to 4.12 present the drop breakup evolution for various flow conditions. In all cases, the Reynolds number in the orifice was maintained at a fixed value ($Re_o = 6800$). There was no evidence of any kind of breakup upstream along the orifice. Although the droplet is deformed by the restriction in the entrance zone, the fragmentation only occurs in the turbulent zone developed downstream of the orifice.

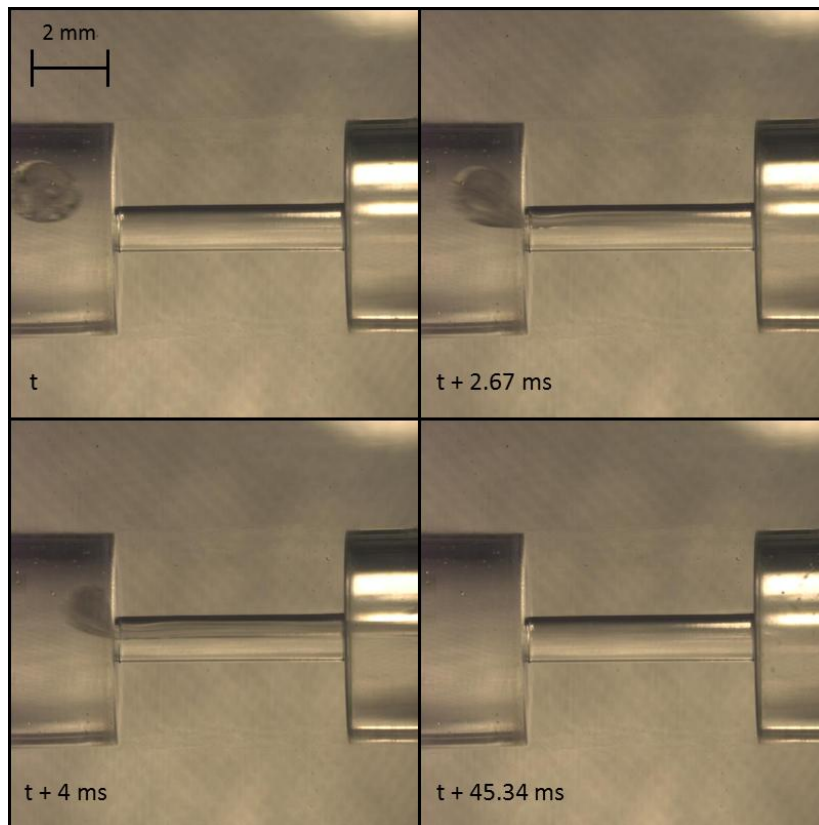


Figure 4. 9 General scheme for turbulent drop breakup through an orifice. $\mu_d = 0.192$

Pa.s, $\sigma = 24.51$ mN/m, $\beta = 0.22$, Orifice Length = 5 mm, $T = 25$ °C.

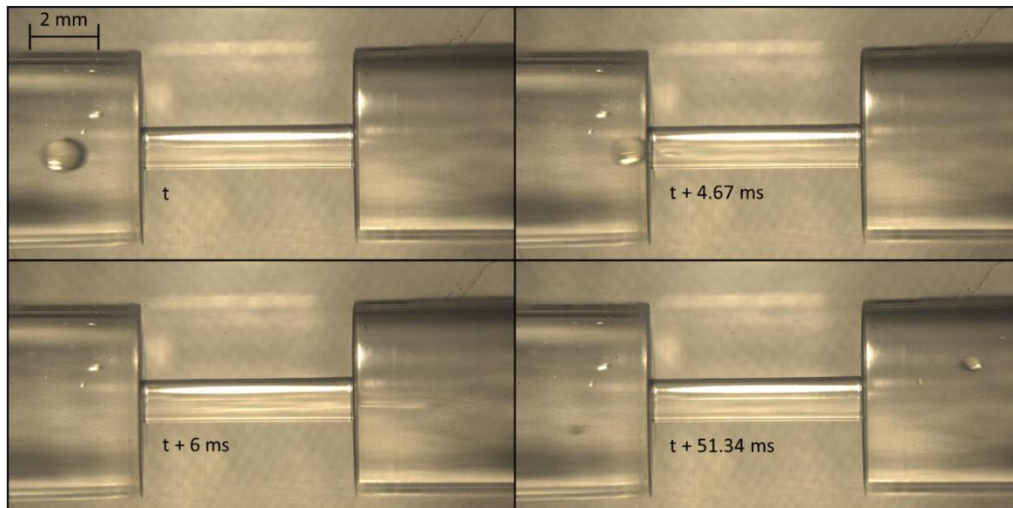


Figure 4. 10 General scheme for turbulent drop breakup through an orifice. $\mu_d = 0.0178$ Pa.s, $\sigma = 17.65$ mN/m, $\beta = 0.22$, Orifice Length = 5 mm, $T = 25$ °C.

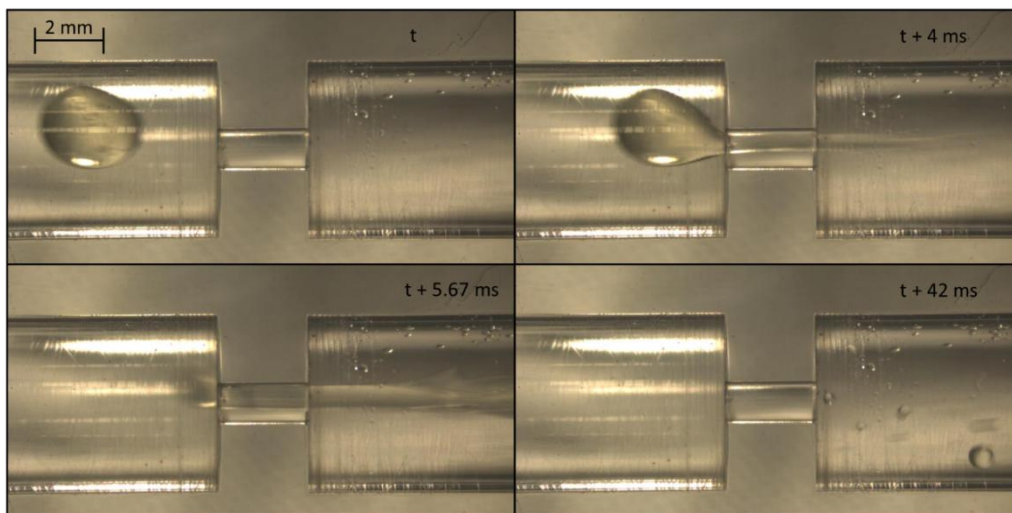


Figure 4. 11 General scheme for turbulent drop breakup through an orifice. $\mu_d = 0.192$ Pa.s, $\sigma = 24.51$ mN/m, $\beta = 0.22$, Orifice Length = 2 mm, $T = 25$ °C.

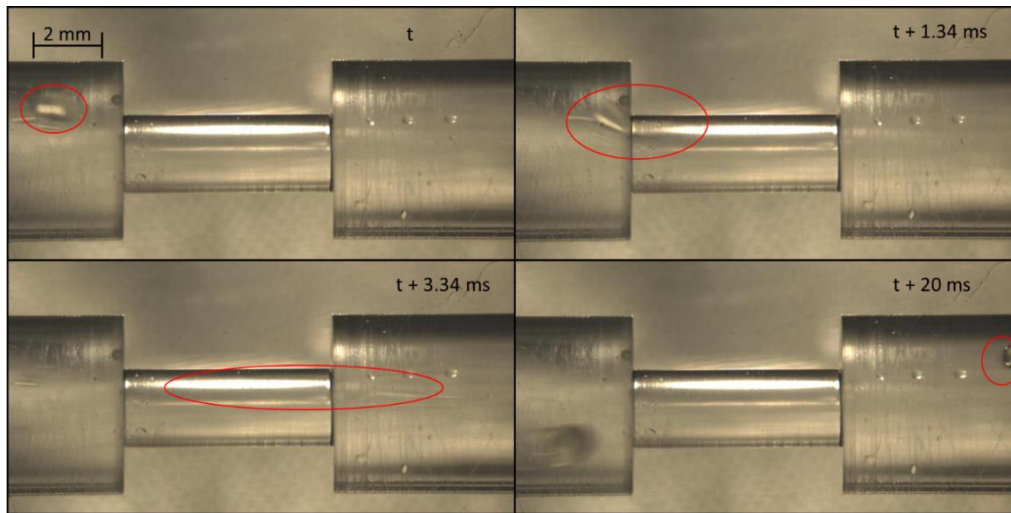


Figure 4.12 General scheme for turbulent drop breakup through an orifice. $\mu_d = 0.192$ Pa.s, $\sigma = 24.51$ mN/m, $\beta = 0.44$, Orifice Length = 5 mm, $T = 25$ °C.

Figure 4.13 shows the evolution of a single droplet breakup occurring downstream of an orifice ($\beta = 0.22$). The oil phase, which is deformed by the restriction, leaves the jet zone as a single drop (Figure 4.13.a). There was no evidence of breakup in the core of the jet zone (Figure 4.13.b). The difference between the velocity in the jet (~ 7 m/s) and the bulk velocity downstream of the orifice (~ 0.3 m/s) causes the droplet deceleration and deformation in the radial direction. The droplet is then exposed to a high velocity gradient as it stretches from the jet zone and the lower velocity flow away from the jet. At some distance from the edge of the restriction (Breakup Length, L_b , Figure 4.13.c), the turbulent stress τ_c (Equation 2.14) overcomes the resistance stresses exerted by the droplet τ_s and τ_d (Equations 2.17 and 2.18 respectively), and finally the drop breaks (Figure 4.13.d). As defined from Equation 2.14, the turbulent stress is a function of the velocity gradient in the flow, which can be axial (in the direction of the flow) or radial. As already stated, there is no breakup in the core of the jet; therefore, the axial gradient of velocity is not responsible for the droplet breakup. Instead of that, it seems to be that the radial gradient of axial velocity is the responsible for starting the fragmentation process, because at L_b , it is large enough to overcome the resistance stresses and produce the droplet breakage. After the drop disintegrates, several “daughter droplets” are generated in specific turbulent regions of the flow (Figure 4.13.e). Some of them will enter in a recirculation zone, where apparently, the deformation stresses are not strong enough to produce additional fragmentation (Figure 4.13.f). In some cases, the flow pattern can carry

the daughter droplets to breakup regions (zones where the radial velocity gradient is large enough to produce breakage), where more daughter droplets are generated. These annotations are in agreement with the previous observations made by Galinat et al. (2005) for the case of drop breakup through an orifice plate. Therefore, from the observations made in this work, it is possible to conclude that the orifice length does not influence the breakup mechanisms.

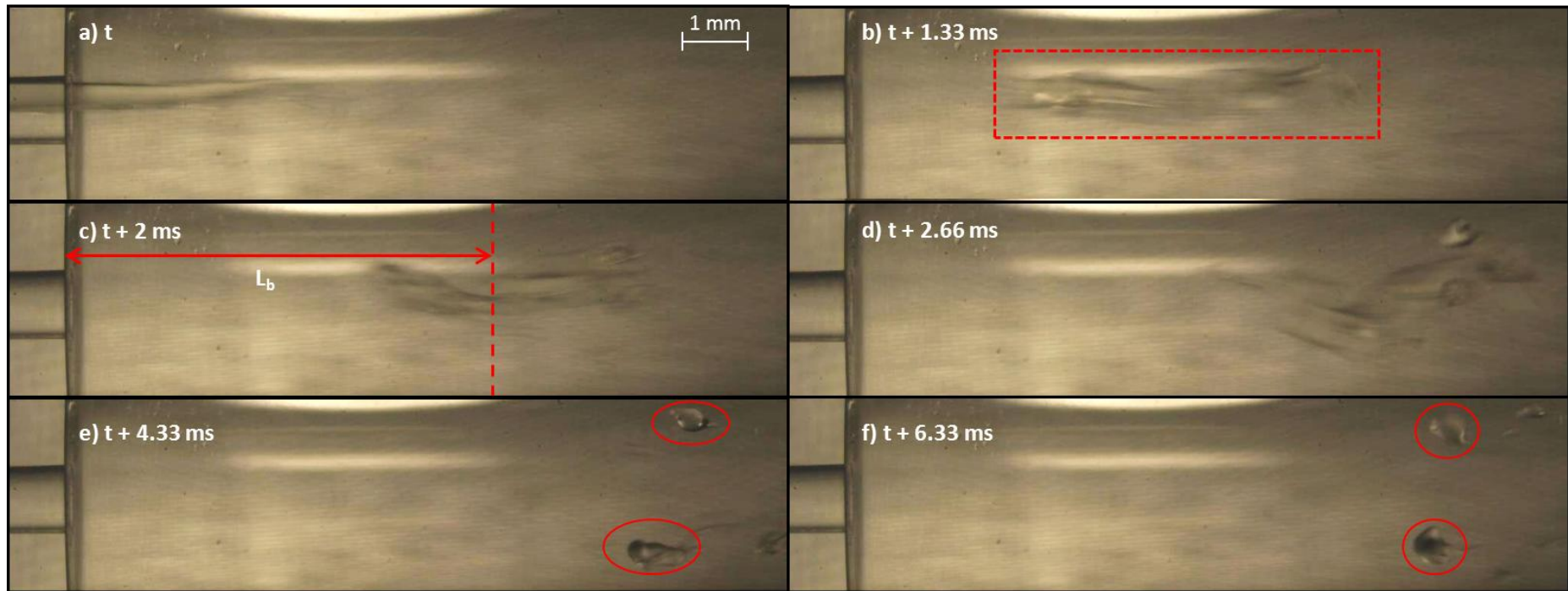


Figure 4. 13 Sequence of turbulent drop breakup downstream of an orifice. $\mu_d = 0.192$ Pa.s, $\sigma = 24.51$ mN/m, $\beta = 0.22$, Orifice Length = 5 mm, $T = 25$ °C.

4.1.2.1 Effect of interfacial tension

As in the case of drop breakup in the rotor – stator mixer (and in general for turbulent drop breakup), larger drop sizes and a lower magnitude of fragmentation are produced with high interfacial tension systems (Figure 4.14) in comparison with low interfacial tension systems (Figure 4.15). It was possible to estimate the breakup length (L_b) for the orifice of 1 mm of intern diameter using image analysis. It was observed that breakup length for high interfacial tension systems is larger (~ 1.8 pipe diameters) than for low interfacial tension systems (~ 1.1 pipe diameters). That occurs because the deformation resistance is larger in high interfacial tension systems, such that the radial velocity gradient required for initial breakup is attained at a larger distance from the edge of the orifice.

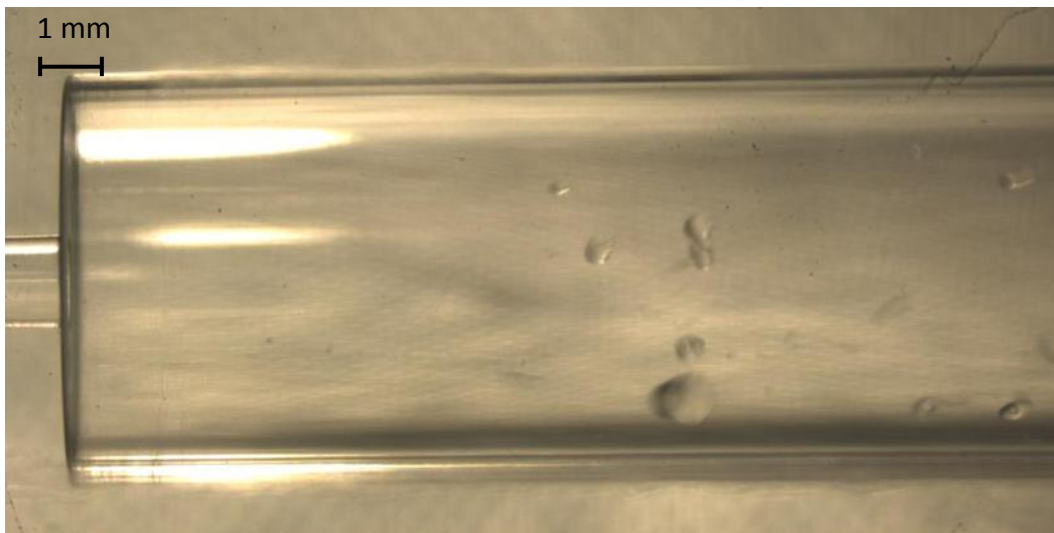


Figure 4. 14 Droplet breakup and initial fragmentation in a high interfacial tension system (14 ms after the initial breakup). $\mu_d = 0.0178$ Pa.s, $\sigma = 17.65$ mN/m, $\beta = 0.22$, Orifice Length = 5 mm, $T = 25$ °C.



Figure 4. 15 Droplet breakup and initial fragmentation in a low interfacial tension system (6 ms after the initial breakup). $\mu_d = 0.0178$ Pa.s, $\sigma = 1.97$ mN/m, $\beta = 0.22$, Orifice Length = 5 mm, $T = 25$ °C.

4.1.2.2 Effect of dispersed phase viscosity

As expected, low fragmentation rate and high equilibrium drop sizes were observed for moderate dispersed phase viscosity systems. According to discussion in section 4.1.1.1.2, this occurs because viscous droplets present a larger resistance to deformation stresses. In this case, a small difference between L_b for moderate (~ 1.8 pipe diameters) and low viscosity droplets (~ 1.6 pipe diameters) was estimated. Consequently, at experimental conditions evaluated in this work, the breakup length depends intensely on the interfacial tension.

4.2 Maximum stable drop diameter correlations

This subsection presents the results corresponding to the experimental MSDD data obtained for the turbulent breakup of diluted (5% of dispersed phase) O/W emulsions in a rotor – stator mixer and through an orifice in a pipe ($\beta = 0.22$, orifice length = 5 mm). Then, the gathered data was correlated to a mechanistic model using a non-linear optimization tool. The mechanistic model was previously used by Wang and Calabrese (1986) to correlate the MSDD obtained

in regular stirred tank contactors, and then by Padron (2005) to correlate the breakup in a Silverson rotor – stator mixer.

4.2.1 MSDD in the rotor – stator mixer

In this case it was assumed that the MSDD was obtained for sufficiently high mixing times. Figure 4.16 shows the evolution of the drop size as a function of the mixing time for different mixing speeds.

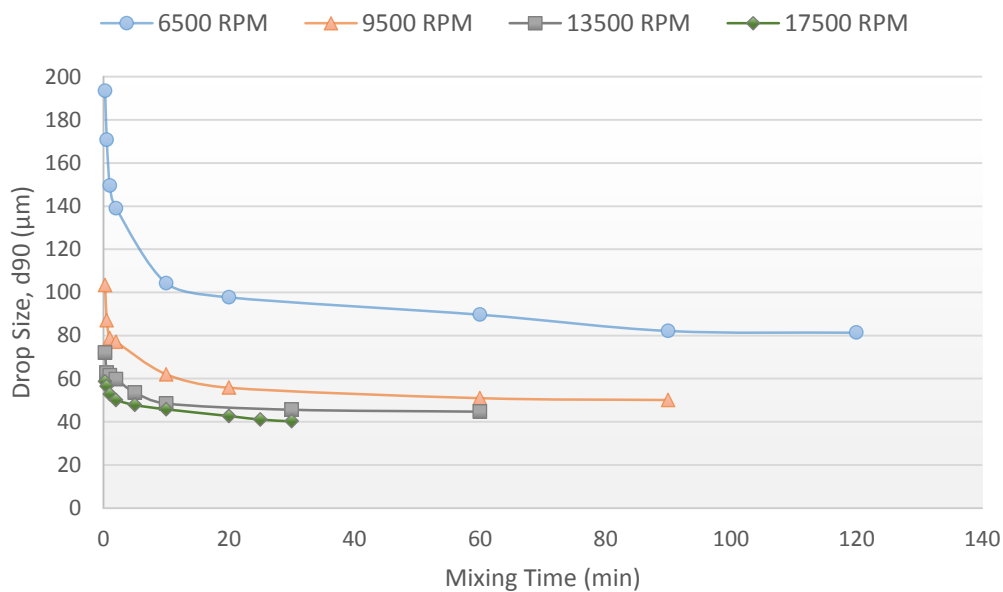


Figure 4. 16 Evolution of the maximum drop size with the mixing time for different mixing speeds in the rotor – stator mixer. $\mu_d = 0.192 \text{ Pa.s}$, $T = 25 \text{ }^\circ\text{C}$.

It can be observed an asymptotical behavior for all mixing speeds at high mixing times (where the magnitude of high mixing time depends on each mixing speed). Consequently, it is possible to assume that the last point in each curve represents the maximum stable drop diameter or it is close to that value.

Then, using Equations 2.25 and 2.10, the energy dissipation rate and the Kolmogorov's length micro scale are calculated, respectively. Figure 4.17 presents the maximum stable drop sizes (d_{90}) obtained for both dispersed phases and the Kolmogorov's micro scale values as functions of the energy dissipation rate. It is observed that always the maximum stable drop sizes are larger than the Kolmogorov's length micro scale. Even using the Sauter mean diameter (d_{32}), the stable drop sizes are larger than the Kolmogorov's length micro scale (Figure

4.18). Therefore, the breakup process in the rotor – stator mixer occurs in the inertial sub-range.

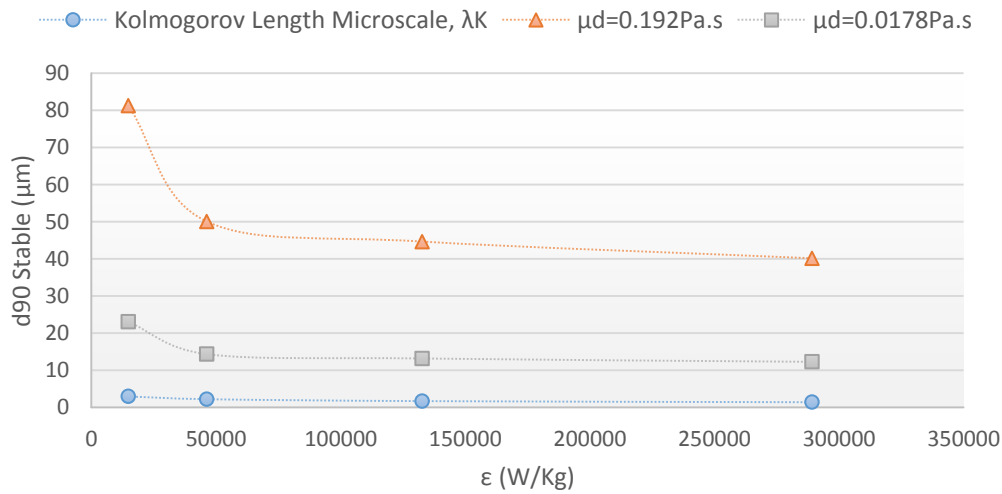


Figure 4. 17 Maximum stable drop diameter (d_{90}) and Kolmogorov's length micro scale for different values of energy dissipation rate per unit mass. Turbulent drop breakup of a 5% O/W emulsion in a rotor – stator mixer. $\sigma = 1.79 - 1.97$ mN/m, $T = 25$ °C.

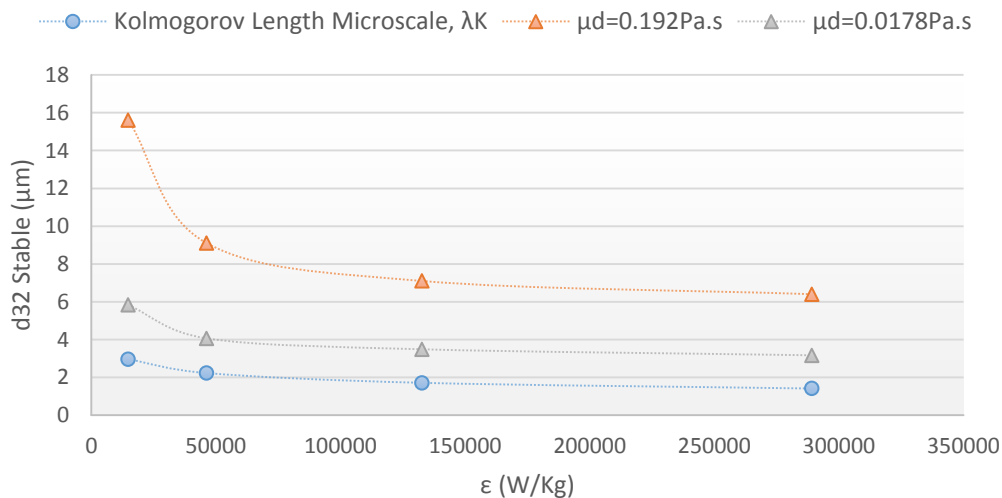


Figure 4. 18 Sauter mean stable drop size (d_{32}) and Kolmogorov's length micro scale for different values of energy dissipation rate per unit mass. Turbulent drop breakup of a 5% O/W emulsion in a rotor – stator mixer. $\sigma = 1.79 - 1.97$ mN/m, $T = 25$ °C.

It was observed that the less viscous oil produces smaller droplet sizes, as explained in section 4.1.1.1.2. In addition, the data showed a decreasing behavior becoming less sensitive for high energy dissipation rates. Experimental conditions for the case of breakup study in a Rotor – Stator Mixer are shown in Table 4.1.

Table 4. 1 Experimental data obtained in MSDD determination for turbulent drop breakup in a rotor – stator mixer.

Mixing Speed (RPM)	Mixing Speed (RPS)	Tip Speed (m/s)	Re (*10 ⁴)	ε (*10 ⁴ , W/Kg)
6500	108.33	4.56	1.86	1.48
9500	158.33	6.66	2.72	4.63
13500	225	9.47	3.87	13.28
17500	291.66	12.27	5.01	28.92

4.2.1.1

Correlations of MSDD to a mechanistic model

The two coefficients of the mechanistic model for inertial sub range (Equations 2.22) were adjusted to the experimental data using a Non-Linear optimization tool based in the Generalized Reduced Gradient code (GRG2). In all cases, the precision of the model was calculated using the Root Mean Squared Difference (RMSD) between experimental and predicted data, as given by Equation 4.1:

$$RMSD = 100 \sqrt{\frac{\sum_i \left(\frac{(d_{90})_{Exp.} - (d_{90})_{Calc.}}{(d_{90})_{Exp.}} \right)_i^2}{N^*}} \quad (4.1)$$

Where N^* is the number of data points. In that way, a lower RMSD value (in %) indicates a higher accuracy for the evaluated correlation.

Equations 4.2 and 4.3 present the correlated linear mechanistic model and the RMSD obtained for both oils, the 500 PS and the Drakeol 7, respectively.

$$d_{90} = 0.25 \left(\frac{\sigma}{\rho_c} \right)^{3/5} \varepsilon^{-2/5} \left[1 + 4.00 \frac{\mu_d}{\sigma} \left(\frac{\rho_c}{\rho_d} \right)^{1/2} \varepsilon^{1/3} d_{90}^{1/3} \right]^{3/5} \\ RMSD = 9.42\% \quad (4.2)$$

$$d_{90} = 0.37 \left(\frac{\sigma}{\rho_c} \right)^{3/5} \varepsilon^{-2/5} \left[1 + 4.07 \frac{\mu_d}{\sigma} \left(\frac{\rho_c}{\rho_d} \right)^{1/2} \varepsilon^{1/3} d_{90}^{1/3} \right]^{3/5} \\ RMSD = 11.22\% \quad (4.3)$$

The two models showed similar values for both coefficients. However, there is a slight difference in C_3 values, indicating that interfacial effects are more important for low viscosity oils than for moderate viscosity oils. The same values obtained for C_4 (related to viscous effects) are explained based in the low to moderate viscosity nature of both oils. Figures 4.19 and 4.20 show the experimental (real) drop sizes, the droplet sizes predicted by the linear mechanistic model (Equations 4.2 and 4.3) and a simple power law linear fitting for the 500 PS and Drakeol 7 oils respectively.

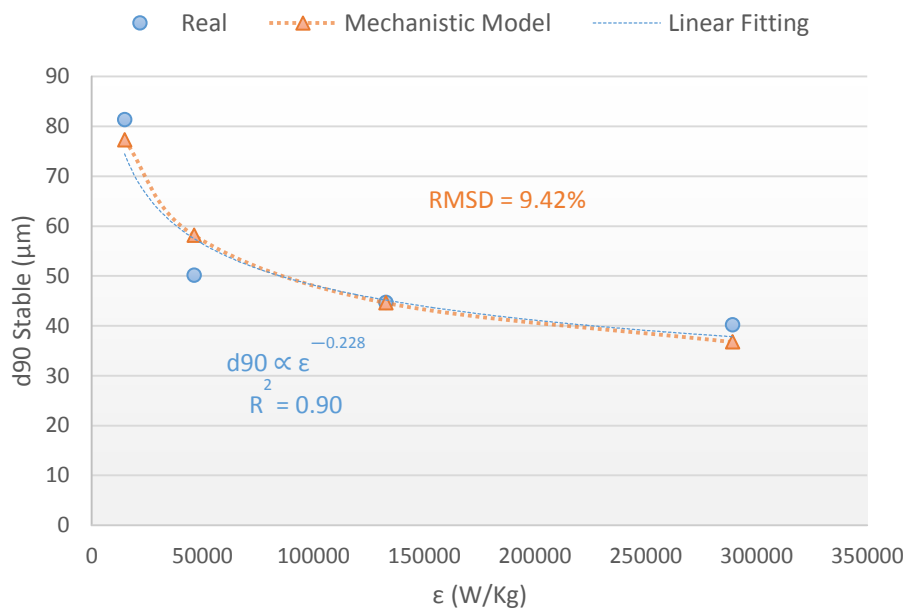


Figure 4. 19 Linear and non-linear curve fittings to MSDD data for turbulent drop breakup of a 5% O/W emulsion in a rotor – stator mixer. $\mu_d = 0.192$ Pa.s, $\sigma = 1.79$ mN/m, $T = 25$ °C.

In this case, the mechanistic models produced reasonable good fittings for both oils, represented in the low RMSD values. However, the linear power law fitting was not quiet good (low correlation coefficients). The linear fitting of the maximum stable droplet size as a function of the energy dissipation rate was almost as if we neglect the term between the brackets (viscous term) is Equations 4.2 and 4.3, remaining only the term related to interfacial effects. The low correlation coefficients and the difference between the determined exponents (-0.228 and -0.203 for 500 PS and Drakeol 7 respectively) and the theoretical power (-0.4), allowed to conclude that breakup process in the rotor – stator mixer is not

entirely dominated by interfacial effects. Instead of that, it is a function of both, interfacial and viscous effects.

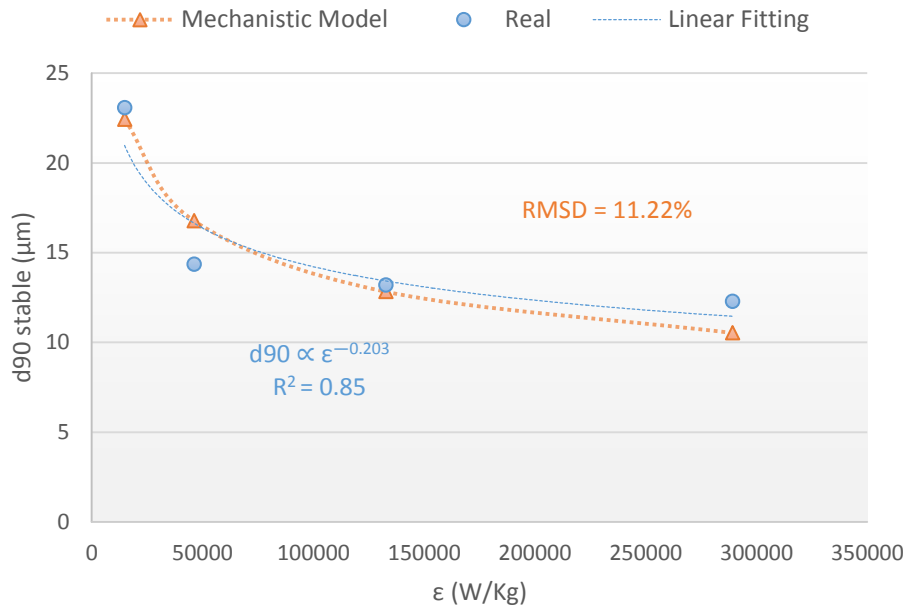


Figure 4. 20 Linear and non-linear curve fittings to MSDD data for turbulent drop breakup of a 5% O/W emulsion in a rotor – stator mixer. $\mu_d = 0.0178$ Pa.s, $\sigma = 1.97$ mN/m, $T = 25$ °C.

4.2.2 MSDD in the flow through an orifice

In this case, the MSDD was determined from the difference between the drop size distributions obtained upstream and downstream of the restriction for the flow of 5% O/W emulsions through an orifice ($\beta = 0.22$, orifice length = 5 mm) using the criterion given by Equation 3.7.

4.2.2.1 Preliminary considerations

The dissipation length (L_{dis}) in Equation 2.27 (required parameter to calculate the average energy dissipation rate per unit mass) was estimated from visualization of a region where no noticeable shear stresses were acting on the droplets. To do that, images obtained from the visualization experiments for the case of turbulent breakup through an orifice were used.

Figure 4.21 represents a description of the L_{dis} determination for a specific flow condition. It was observed that only the final portion of the transparent device presented visual evidence of an energy dissipation frontier (Figure 4.21.a). It is possible to note a zone where daughter droplets are suddenly returning to their spherical form (Figure 4.21.b), which means that droplets are suffering an abrupt deceleration. Most of the drops stop near that region (Figure 4.21.c). Therefore, turbulent stresses are not acting on the droplets and that zone can be considered as a limit region for energy dissipation (Figure 4.21.d).

Then, the dissipation length was estimated from the design of the device (Figure 4.22) and simple image analysis techniques for various flow cases. Table 4.2 summarizes and compares the calculated values to numerical predictions obtained by van der Zande (2000) for drop breakup through a restriction in a pipe of 4.5 mm of internal diameter (Figure 4.23).

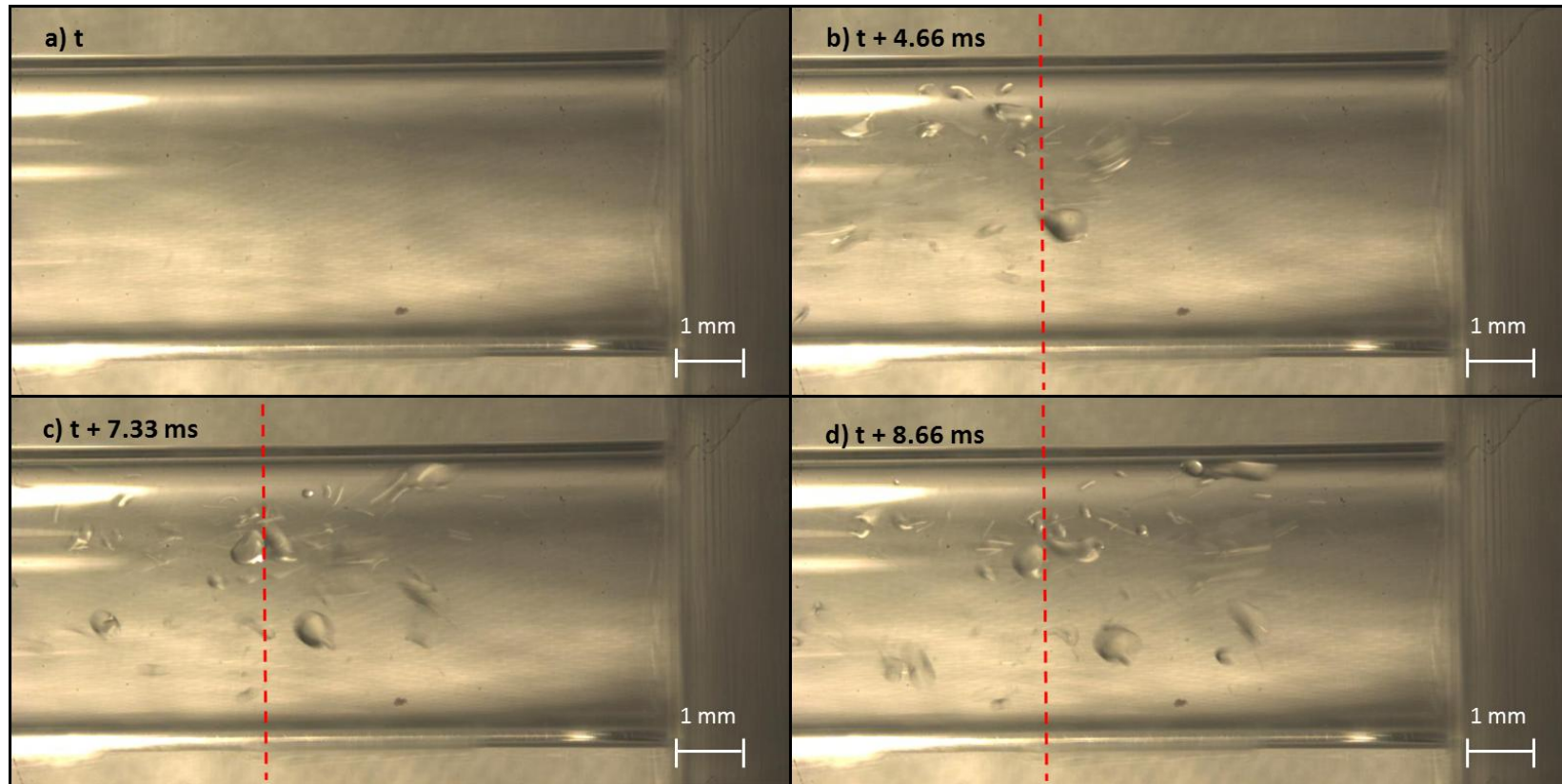


Figure 4. 21 Visual Estimation of Dissipation Length. $\mu_d = 0.192$ Pa.s, $\sigma = 1.79$ mN/m, $\beta = 0.22$, Orifice Length = 5 mm, $T = 25$ °C.

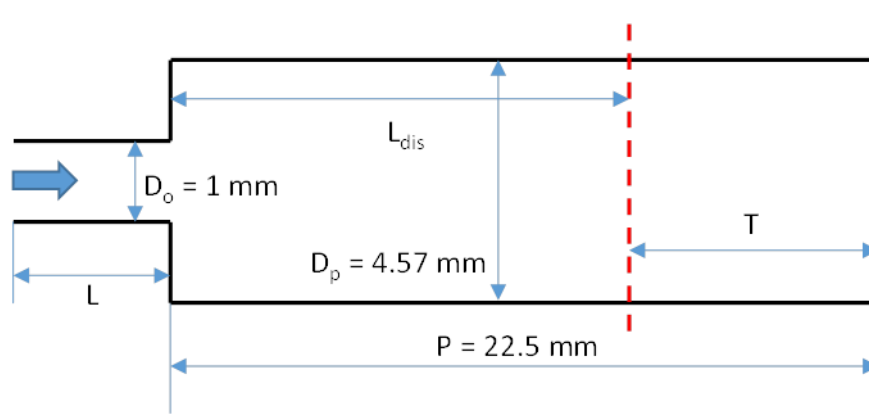


Figure 4.22 Typical dimensions of the transparent device used for estimation of dissipation length.

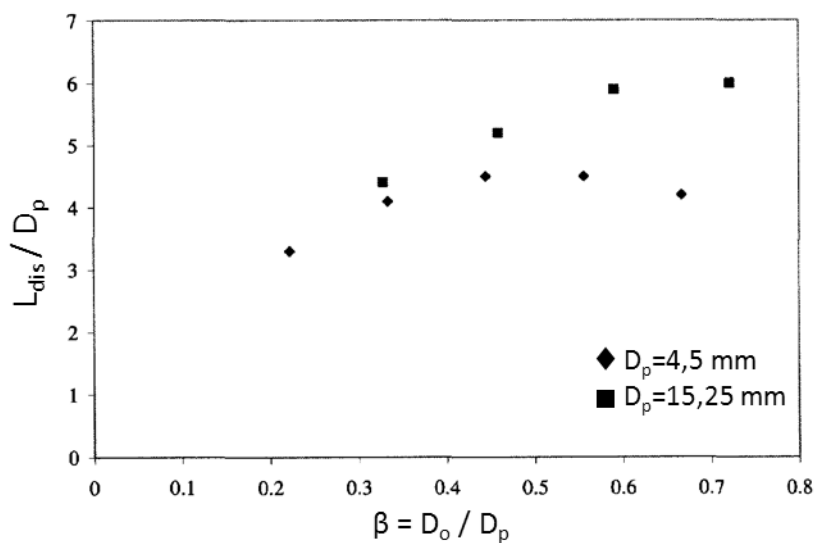


Figure 4.23 The length of dissipation zone versus β , the ratio between the orifice diameter and the pipe diameter. The dissipation length has been scaled with the pipe diameter. Adapted from van der Zande, 2000.

Table 4.2 Calculated dissipation length from visualization experiments and from numerical simulations by van der Zande, 2000.

Case	μ_d (Pa.s)	Continuous Phase	D_o (mm)	L (mm)	T (mm)	L_{dis} Calc. (mm)	L_{dis} vdZ (mm)
I	0.192	Tap Water	1	5	7.613	14.887	15.081
II	0.192	Surf. Based	1	5	7.28	15.22	15.081
III	0.0178	Surf. Based	1	5	7.307	15.193	15.081
IV	0.192	Tap Water	1	2	7.436	15.064	15.081
V	0.192	Tap Water	2	2	3.905	18.595	19.198

The similarity between the estimated values from the visualization technique and the calculated values by van der Zande allowed to use them as a base for calculation of the average energy dissipation rate (Equation 2.25) and the Kolmogorov's length micro scale (Equation 2.12).

4.2.2.2 Experimental MSDD data

Table 4.3 shows the energy dissipation rate and Kolmogorov's length micro scale values calculated using the dissipation length values found in section 4.2.2.1 for the different experimental conditions evaluated in the MSDD experiments. Figures 4.24 to 4.27 show the typical charts for MSDD determination for different flow conditions as explained in Table 4.3. The black line represents a zero breakup probability line; meanwhile, blue and orange series represent the data for both evaluated oils. In each figure, the d_{90} upstream of the orifice is plotted against the d_{90} downstream of the orifice. The MSDD is obtained when the criterion given by Equation 3.7 is satisfied.

Table 4. 3 Experimental data obtained in MSDD determination for turbulent drop breakup through an orifice.

Flow Case	Total Flow Rate, Q_T (L/min)	Velocity in the Orifice, U_o (m/s)	Reynolds Number in the Orifice, Re_o ($*10^3$)	Permanent Pressure Drop, Δp_{perm} ($*10^4$, Pa)	Average Energy Dissipation Rate, ε ($*10^4$, W/Kg)	Kolmogorov's Length Micro scale, λ_K (μm)
1	0.488	10.36	9.93	4.94	3.29	2.423
2	0.658	13.96	13.38	8.83	7.94	1.945
3	0.817	17.34	16.61	13.53	15.11	1.656
4	0.976	20.71	19.85	18.91	25.23	1.457

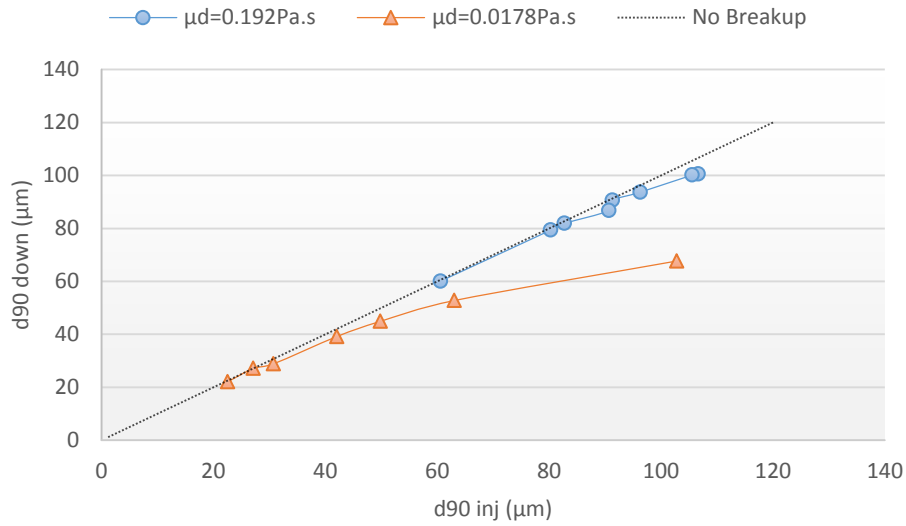


Figure 4. 24 Determination of MSDD for turbulent breakup through an orifice. Flow case 1. $\varepsilon = 3.29 \cdot 10^4$ W/Kg.

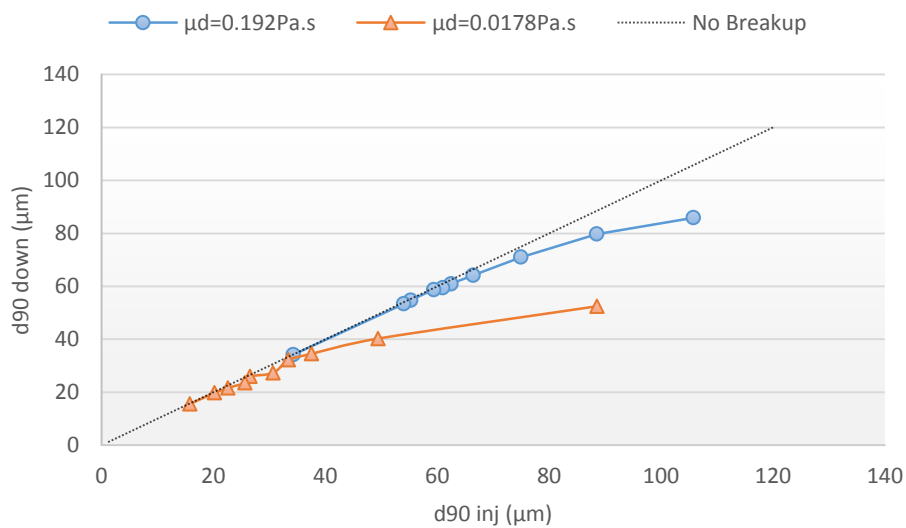


Figure 4. 25 Determination of MSDD for turbulent breakup through an orifice. Flow case 2. $\varepsilon = 7.94 \cdot 10^4$ W/Kg.

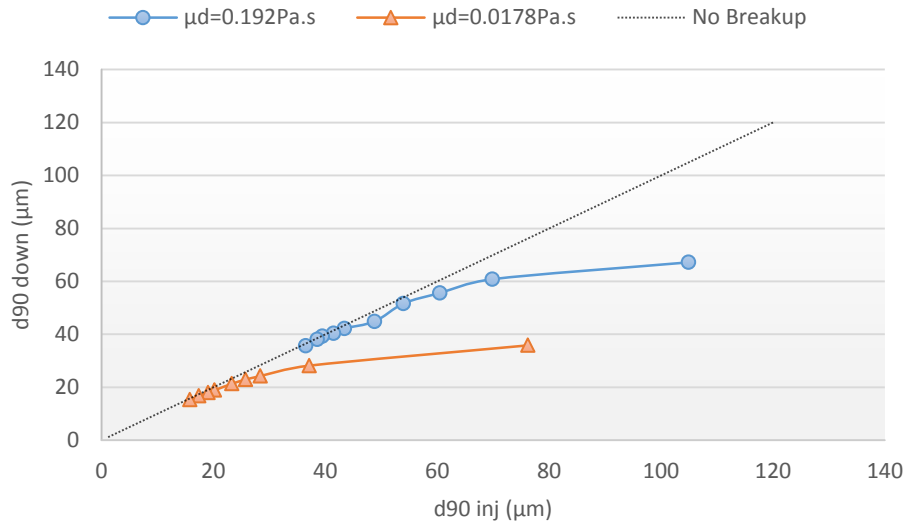


Figure 4. 26 Determination of MSDD for turbulent breakup through an orifice. Flow case 3. $\varepsilon = 15.11 \cdot 10^4 \text{ W/Kg}$.

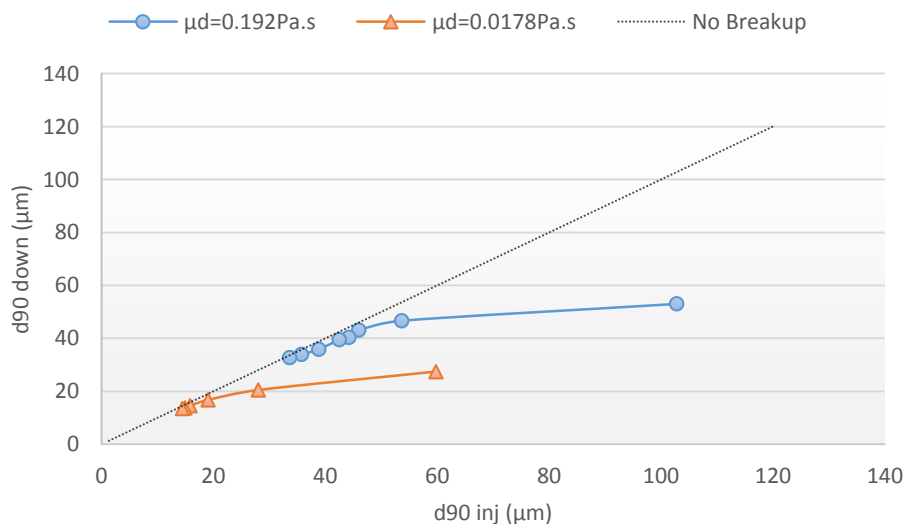


Figure 4. 27 Determination of MSDD for turbulent breakup through an orifice. Flow case 4. $\varepsilon = 25.23 \cdot 10^4 \text{ W/Kg}$.

It is important to note that for high Reynolds number (Figure 4.26 and Figure 4.27) the dependence of d_{90} downstream of the orifice is low when $d_{90} \text{ inj} > MSDD$. The latter means that for a high dissipation rate, the fragmentation rate is higher, leading to an intense breakup. Figure 4.28 reports the MSDD values as a function of the energy dissipation rate per unit mass for both evaluated oils and the Kolmogorov's length micro scale values. As in the case of the mixer, the experimental maximum stable drop sizes (d_{90}) were always larger

than the Kolmogorov's length micro scale but smaller than the characteristic length of the flow (L , the orifice diameter). Even the experimental maximum Sauter mean diameter (surface-volume mean diameter, d_{32}) values meet that requirement (Figure 4.29). For that reason, as in the case of the rotor – stator mixer, the drop breakup process through the orifice can be described according to the theoretical considerations of the inertial sub range.

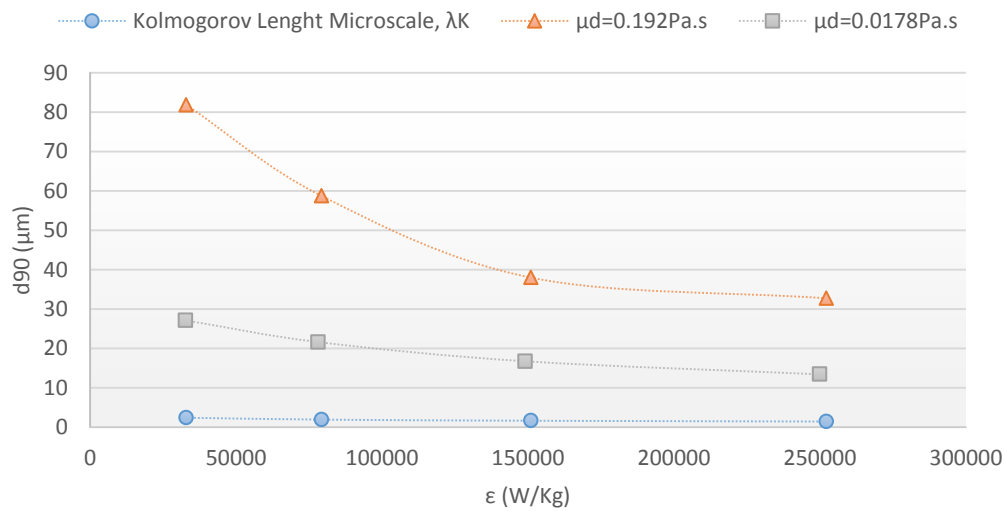


Figure 4. 28 Maximum stable drop diameter and Kolmogorov's length micro scale for different values of energy dissipation rate per unit mass. Turbulent drop breakup of a 5% O/W emulsion through an orifice. $\sigma = 1.79 - 1.97 \text{ mN/m}$, $\beta = 0.22$, Orifice Length = 5 mm, $T = 25 \text{ }^\circ\text{C}$.

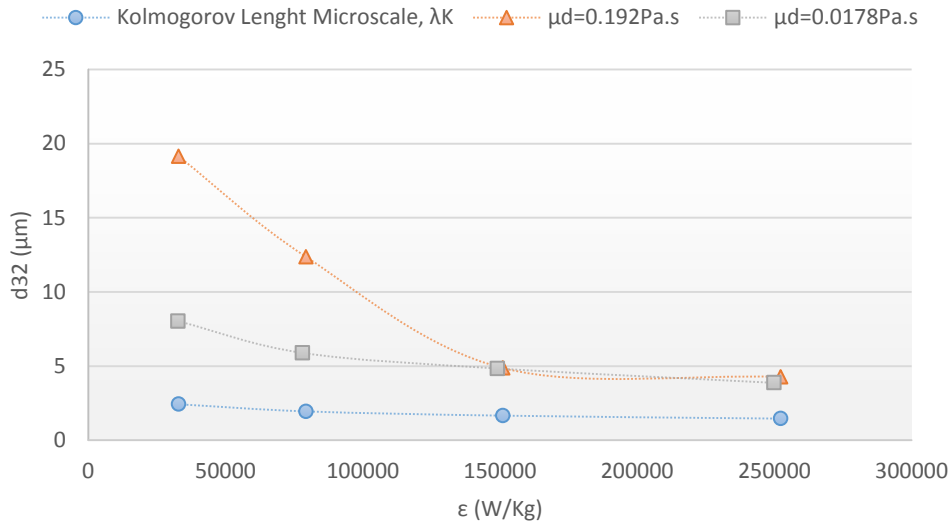


Figure 4. 29 Maximum stable Sauter mean diameter and Kolmogorov's length micro scale for different values of energy dissipation rate per unit mass. Turbulent drop Breakup of a 5% O/W emulsion through an orifice. $\sigma = 1.79 - 1.97$ mN/m, $\beta = 0.22$, Orifice Length = 5 mm, $T = 25$ °C.

As in the case of the mixer, it was also observed that the less viscous oil produces smaller droplet sizes and that the data showed a decreasing behavior becoming less sensitive for high energy dissipation rates.

4.2.2.3 Correlation of MSDD data to a mechanistic model

Equations 4.4 and 4.5 present the correlated linear mechanistic model for both oils, the 500PS and the Drakeol 7, respectively.

$$d_{90} = 0.27 \left(\frac{\sigma}{\rho_c} \right)^{3/5} \bar{\varepsilon}^{-2/5} \left[1 + 4.00 \frac{\mu_d}{\sigma} \left(\frac{\rho_c}{\rho_d} \right)^{1/2} \bar{\varepsilon}^{1/3} d_{90}^{1/3} \right]^{3/5}$$

$$RMSD = 21.82 \%$$
(4.4)

$$d_{90} = 0.49 \left(\frac{\sigma}{\rho_c} \right)^{3/5} \bar{\varepsilon}^{-2/5} \left[1 + 4.05 \frac{\mu_d}{\sigma} \left(\frac{\rho_c}{\rho_d} \right)^{1/2} \bar{\varepsilon}^{1/3} d_{90}^{1/3} \right]^{3/5}$$

$$RMSD = 12.36 \%$$
(4.5)

Again, the same slight difference in C_3 values observed for the model describing the breakup in the mixer indicates that interfacial effects are more important for low viscosity oils than for moderate viscosity oils. In the moderate viscosity case, the RMSD value was higher than the case of the mixer, indicating a lower precision of the models and a worse fitting of the experimental data.

Figures 4.30 and 4.31 show the linear mechanistic model fitting and a simple power law linear fitting for 500PS and Drakeol 7 oils, respectively.

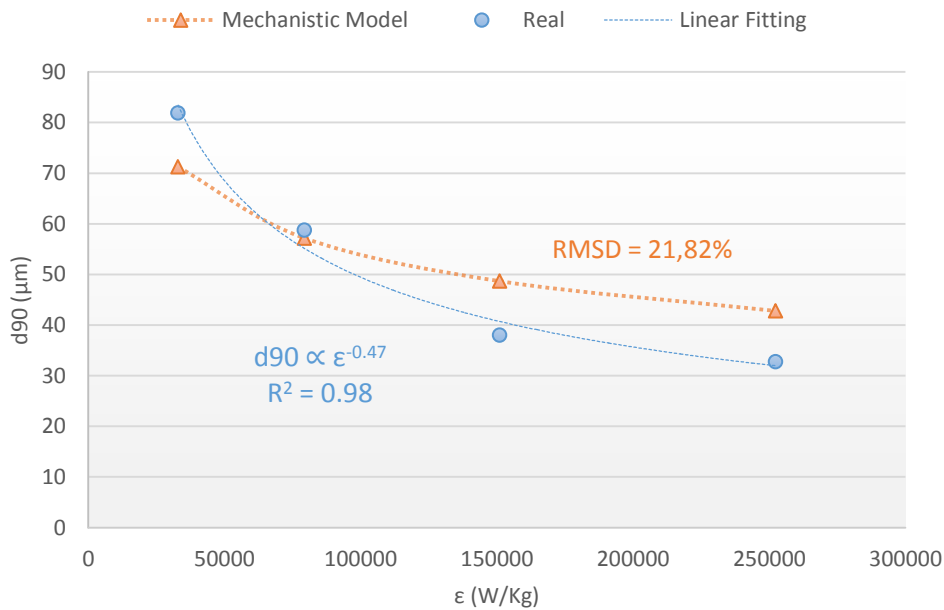


Figure 4. 30 Linear and non-linear curve fittings to MSDD data for turbulent drop Breakup of a 5% O/W emulsion through an orifice. $\mu_d = 0.192$ Pa.s, $\sigma = 1.79$ mN/m, $\beta = 0.22$, Orifice Length = 5 mm, T = 25 °C.

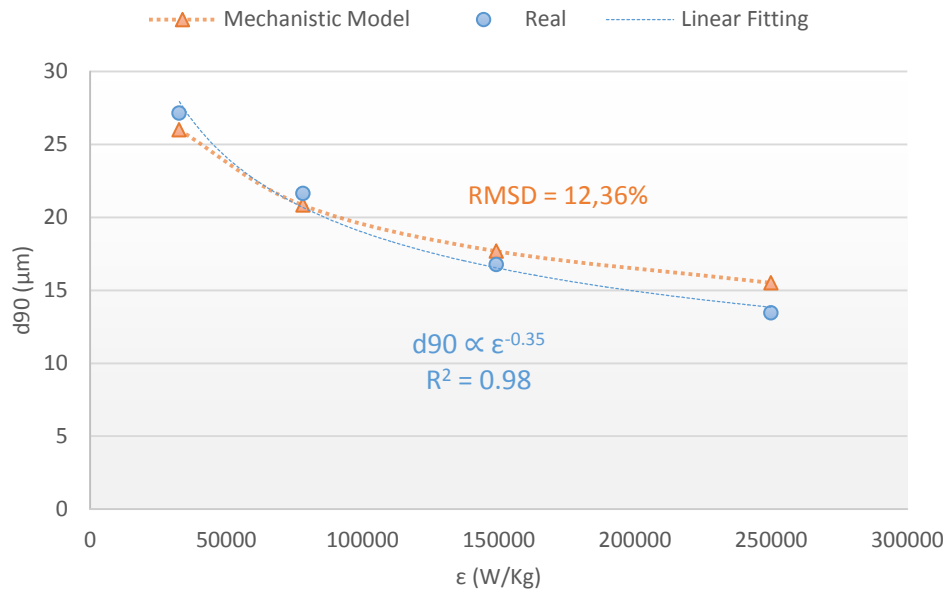


Figure 4. 31 Linear and non-linear curve fittings to MSDD data for turbulent drop breakup of a 5% O/W emulsion through an orifice. $\mu_d = 0.0178$ Pa.s, $\sigma = 1.97$ mN/m, $\beta = 0.22$, Orifice Length = 5 mm, $T = 25$ °C.

The relative low precision of the models lies in the lack of consideration of the time scale required for the breakup (duration of the deforming stress), which is more important in this case than in the case of breakup in the mixer. It must be remembered that in the case of the mixer, the MSDD was obtained for sufficiently high mixing time, reducing the relative importance of the time scale.

For viscous droplets, the influence of the duration of the deformation stress is of greater concern, because their considerable internal viscous stress resists deformation, increasing the time required to reach the drop's critical deformation. Therefore, even if turbulent stress is large enough in magnitude to overcome interfacial and viscous stresses, if it is not imposed for sufficient time, the drop may not break. This fact explains why the model is more accurate for the lower viscosity oil case.

It was also observed that obtained exponents for the average energy dissipation rate per unit mass for power law fitting were close to the exponent for the inviscid case (-0.4). The latter indicates that interfacial effects drive the breakup process in the restriction for low viscosity oils.

It is worth emphasizing that there are no records about the use of this type of mechanistic models in the description of the breakup process through orifices,

therefore, this work represents the first attempt to use them to correlate the maximum stable drop diameter data obtained in this process. The similarity of the C_3 and C_4 coefficients found for the model in both geometrical cases (See Table 4.4), allows to have a rough approximation of the maximum stable drop size that will be obtained in the breakup through the orifice from drop size data at equivalent energy dissipation rates in the rotor – stator mixer.

Table 4. 4 Comparison of Parameters obtained for the Linear Mechanistic Model.

Drop Breakup Case	$\bar{\epsilon}$ Definition	Mechanistic Model	Dispersed Phase Viscosity (Pa.s)	C_3	C_4	RMSD (%)
Rotor – Stator Mixer	$\bar{\epsilon} = \frac{(\pi DN)^3}{4a}$	Linear, Inertial Sub-range	0.192	0.25	4.00	9.42
			0.0178	0.37	4.07	11.22
Orifice in a pipe	$\bar{\epsilon} = \frac{\Delta p_{perm} U_o}{\rho_c L_{dis}}$		0.192	0.27	4.00	21.82
			0.0178	0.49	4.05	12.36